Chemical Science

ROYAL SOCIETY OF CHEMISTRY

EDGE ARTICLE

View Article Online
View Journal | View Issue

Cite this: *Chem. Sci.*, 2023, **14**, 2399

All publication charges for this article have been paid for by the Royal Society of Chemistry

Site-specific covalent metalation of DNA oligonucleotides with phosphorescent platinum(II) complexes†

Felix Boisten,[a] Iván Maisuls, [ab] Tim Schäfer, [a] Cristian A. Strassert [abc]* and Jens Müller [ac]*

Phosphorescent Pt(II) complexes, composed of a tridentate N^N^C donor ligand and a monodentate ancillary ligand, were covalently attached to DNA oligonucleotides. Three modes of attachment were investigated: positioning the tridentate ligand as an artificial nucleobase *via* a 2′-deoxyribose or a propane-1,2-diol moiety and orienting it towards the major groove by appending it to a uridine C5 position. The photophysical properties of the complexes depend on the mode of attachment and on the identity of the monodentate ligand (iodido *vs.* cyanido ligand). Significant duplex stabilization was observed for all cyanido complexes when they are attached to the DNA backbone. The luminescence strongly depends on whether a single or two adjacent complexes are introduced, with the latter showing an additional emission band indicative of excimer formation. The doubly platinated oligonucleotides could be useful as ratiometric or lifetime-based oxygen sensors, as the green photoluminescence intensities and average lifetimes of the monomeric species are drastically boosted upon deoxygenation, whereas the red-shifted excimer phosphorescence is nearly insensitive to the presence of triplet dioxygen in solution.

Received 25th October 2022
Accepted 26th January 2023

DOI: 10.1039/d2sc05916a

rsc.li/chemical-science

Introduction

Nucleic acids represent excellent scaffolds for the predictable arrangement of functional entities in three-dimensional space, making use of their modular composition, their facile modification and their superb self-assembly.[1] This has enabled, amongst others, the field of DNA-templated organic synthesis.[2] Organic chromophores represent another prominent type of moieties assembled using nucleic acids.[3–6] The site-specific incorporation of transition metal ions is of interest, too, because it can equip the DNA with metal-based properties such as luminescence. It is typically achieved by introducing metal-mediated base pairs.[7–9] In this type of artificial base pairs, two ligand-based nucleosides are located on opposing positions within a duplex composed of otherwise complementary oligonucleotides. The respective metal ion then site-specifically binds to this high-affinity binding site.[10,11] While the resulting metal-modified DNA may be fluorescent (depending on the identity of ligand and metal ion),[12] phosphorescent metal complexes have not yet been incorporated into the base pair stack of nucleic acid duplexes. A few examples are known where a luminescent complex is covalently attached to the uridine C5-position, positioning it in the major groove of the duplex.[13,14] In the past, a variety of luminescent intercalating metal complexes have been established, with fascinating applications in optical microscopy.[15–18] Moreover, terminally appended photo-reactive Ru(II) and Rh(III) complexes have been prominently applied,[19] *e.g.* in the study of charge transfer along DNA duplexes.[20] Several organometallic metal-mediated base pairs have also been reported in the context of Hg(II) and Pd(II) complexes.[21–28] Their advantage over regular metal-mediated base pairs is the increased metal–ligand bond strength, so that they persist even at low concentrations.

We report herein on the site-specific covalent incorporation of phosphorescent Pt(II) complexes into DNA duplexes (Chart 1). The coordination compounds are derived from a recently established family of Pt(II) complexes containing a tridentate N^N^C donor ligand and an ancillary monodentate ligand. These species show robust phosphorescence, with an emission wavelength essentially independent of the identity of the monodentate ligand.[29–31] While their green phosphorescence

[a]*Westfälische Wilhelms-Universität Münster, Institut für Anorganische und Analytische Chemie, Corrensstr. 28/30, 48149 Münster, Germany. E-mail: ca.s@uni-muenster.de; mueller.j@uni-muenster.de*

[b]*Westfälische Wilhelms-Universität Münster, Center for Nanotechnology (CeNTech), Heisenbergstr. 11, 48149 Münster, Germany*

[c]*Westfälische Wilhelms-Universität Münster, Center for Soft Nanoscience (SoN) and Cells in Motion Interfaculty Centre (CiMIC), Corrensstr. 28/30, 48149 Münster, Germany*

† Electronic supplementary information (ESI) available: Additional DNA melting curves and CD spectra; lists of melting temperatures; MALDI-ToF spectra; photoluminescence spectra; time-resolved photoluminescence decay curves with fitting parameters; photoluminescence lifetimes; experimental details; NMR spectra. See DOI: https://doi.org/10.1039/d2sc05916a

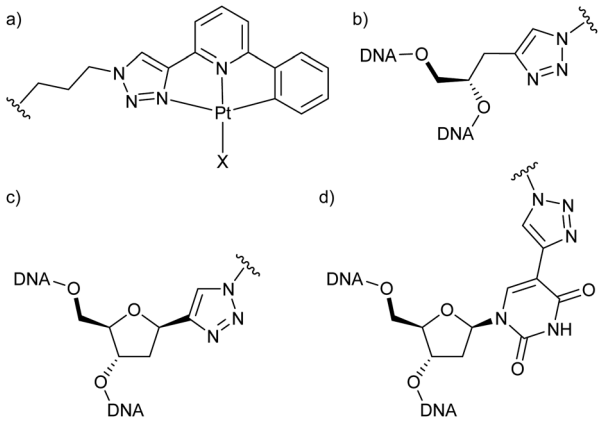

Chart 1 (a) Structure of the Pt(II) complexes used in this study (X = I, CN) and their different modes of attachment to the oligonucleotide *via* (b) a GNA moiety, (c) a 2′-deoxyribose, (d) C5-modified 2′-deoxyuridine.

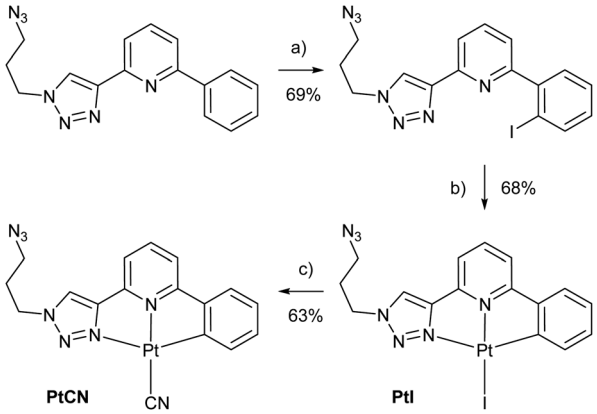

Scheme 1 Synthesis of the Pt(II) precursor complexes **PtI** and **PtCN** for the subsequent cycloaddition to a suitably alkyne-modified oligonucleotide. (a) NIS, $Pd(OAc)_2$, CH_3CN, 90 °C, 2 d; (b) $Pt_2(dba)_3$, THF, 50 °C, 90 min; (c) KCN, CH_3OH/CH_3CN (1 : 1), 90 °C, 3 h. For further synthetic details, see ESI.†

(lifetimes and intensities) is quenched by triplet dioxygen ($^3O_2$), their dimers and higher aggregates appear with a red-shifted yet oxygen-insensitive luminescence portraying excimeric character supported by metal–metal interactions (*i.e.*, coupling between d_{z^2}-orbitals protruding out of the coordination plane). The site-specific incorporation of a Pt(II) complex into DNA is complicated by the high affinity of Pt(II) for purine N7 positions, as is well-known from the mode of action of the antitumor drug cisplatin.[32] In the past, two pre-platinated building blocks for automated DNA solid-phase synthesis were reported to tackle this challenge.[33,34] Similarly, the solid-phase synthesis of a terminally Pt(II)-modified oligonucleotide was reported.[35] However, none of these approaches can be applied for the introduction of the Pt(II) complex under consideration here, because they make use of exclusively monodentate ligands. Instead, we decided to use the Cu(I)-catalysed azide–alkyne Huisgen cycloaddition to achieve the desired site-specific attachment of the Pt(II) complexes. A similar approach was recently reported in the context of (non-luminescent) *cis*-Pt(II)-modified triplex-forming oligonucleotides.[36]

Results and discussion

Synthesis and nomenclature

To be able to compare different locations of the Pt(II) complex within the DNA duplex, three points of attachment were evaluated: (a) *via* a glycol nucleic acid (GNA) moiety, (b) *via* a 2′-deoxyribose and (c) *via* a C5-alkynylated 2′-deoxyuridine moiety (Chart 1). The Pt(II) precursor complexes **PtI** and **PtCN** were prepared *via* oxidative addition (and subsequent ligand exchange in the case of **PtCN**) using a suitably iodinated ligand precursor (Scheme 1). These precursor complexes were attached to the respective oligonucleotides in a post-synthetic Cu(I)-catalysed azide–alkyne Huisgen cycloaddition (see ESI† for details). Table 1 summarizes the DNA duplexes under investigation in this study. It is essentially one duplex sequence with a variable central base pair. All four canonical nucleobases are placed opposite the artificial one. Taking into consideration the two Pt(II) complexes (**PtI**, **PtCN**) and the three modes of attachment (GNA, Chart 1b; DNA, Chart 1c; Uri, Chart 1d), 20 duplexes with a single site-specific Pt(II) modification were prepared, plus eight reference duplexes in which the Pt(II)-containing GNA or DNA building blocks were replaced by an unsubstituted 1*H*-1,2,3-triazole-4-yl base (tri). Throughout the herein reported work, the identity of the Pt(II) complex and its mode of attachment are designated using a superscript denotation. For example, $\mathbf{II}^{\mathbf{PtCN,GNA}}$ represents duplex **II** (with a cytosine opposite the artificial nucleobase) bearing a **PtCN** complex attached *via* a GNA moiety. Similarly, $ODN1^{Tri,DNA}$ represents a single-stranded oligonucleotide with a central non-platinated 1*H*-1,2,3-triazole attached *via* a 2′-deoxyribose. In addition, duplex **V** was prepared, bearing two centrally located consecutive **PtCN** complexes (connected *via* a 2′-deoxyribose) and two complementary guanine residues.

Characterization of duplex stability and conformation

DNA melting studies were initially performed with all duplexes in which the Pt(II) complexes are attached directly to the DNA

Table 1 DNA duplexes under investigation in this study[a]

Duplex		Sequence
$\mathbf{I}^{\mathbf{X}}$	$ODN1^{X}$	5′-d(CTT TCT XTC CCT C)-3′
	$ODN2^{G}$	3′-d(GAA AGA GAG GGA G)-5′
$\mathbf{II}^{\mathbf{X}}$	$ODN1^{X}$	5′-d(CTT TCT XTC CCT C)-3′
	$ODN2^{C}$	3′-d(GAA AGA CAG GGA G)-5′
$\mathbf{III}^{\mathbf{X}}$	$ODN1^{X}$	5′-d(CTT TCT XTC CCT C)-3′
	$ODN2^{A}$	3′-d(GAA AGA AAG GGA G)-5′
$\mathbf{IV}^{\mathbf{X}}$	$ODN1^{X}$	5′-d(CTT TCT XTC CCT C)-3′
	$ODN2^{T}$	3′-d(GAA AGA TAG GGA G)-5′
V	$ODN3^{X}$	5′-d(CTT TCT XXC CCT C)-3′
	ODN4	3′-d(GAA AGA GGG GGA G)-5′

[a] The letter **X** represents the identity of the Pt(II) complex and its point of attachment (**PtI**, **PtCN**, GNA, DNA, Uri). In Pt(II)-free reference duplexes, an unsubstituted 1,2,3-triazole moiety (Tri) was used. See text for more details.

Table 2 Melting temperature T_m/°C and change in melting temperature ΔT_m/°C compared to $I^{Tri,GNA}$–$IV^{Tri,GNA}$ and $I^{Tri,DNA}$–$IV^{Tri,DNA}$, respectively[a]

Duplex	T_m	ΔT_m	Duplex	T_m	ΔT_m
$\mathbf{I}^{Tri,GNA}$	26.1	n.a.	$\mathbf{I}^{Tri,DNA}$	30.5	n.a.
$\mathbf{I}^{PtI,GNA}$	19.9	−6.2	$\mathbf{I}^{PtI,DNA}$	13.8	−16.7
$\mathbf{II}^{Tri,GNA}$	24.3	n.a.	$\mathbf{II}^{Tri,DNA}$	28.1	n.a.
$\mathbf{II}^{PtI,GNA}$	19.0	−5.3	$\mathbf{II}^{PtI,DNA}$	11.6	−16.5
$\mathbf{III}^{Tri,GNA}$	28.2	n.a.	$\mathbf{III}^{Tri,DNA}$	31.3	n.a.
$\mathbf{III}^{PtI,GNA}$	20.4	−7.8	$\mathbf{III}^{PtI,DNA}$	12.2	−19.1
$\mathbf{IV}^{Tri,GNA}$	25.0	n.a.	$\mathbf{IV}^{Tri,DNA}$	27.7	n.a.
$\mathbf{IV}^{PtI,GNA}$	19.1	−5.9	$\mathbf{IV}^{PtI,DNA}$	11.8	−15.9

[a] Experimental conditions: 1 μM DNA duplex, 5 mM MOPS buffer (pH 7.0), 150 mM $NaClO_4$, 2.5 mM $Mg(ClO_4)_2$.

backbone, *i.e., via* the GNA or the 2′-deoxyribose linker. All duplexes bearing a **PtI** complex show a broad melting transition and a melting temperature T_m significantly below that of the corresponding Pt(II)-free reference duplexes (Table 2 and Fig. S1†). Nevertheless, the duplexes mainly adopt a regular B-DNA-type geometry, as indicated by their CD spectra (Fig. S2†). The destabilization is even more pronounced for the duplexes in which a 2′-deoxyribose linker is used to attach the Pt(II) complex. The broad melting transition could be explained by the loss of the iodido ligand, followed by a non-specific complexation of one of the canonical nucleobases, either in an intrastrand or an interstrand fashion. As numerous nucleobases are available for this platination, different products are expected, all of which melt at different temperatures. The resulting duplexes are expected to be distorted, thereby explaining the decrease in T_m. The fact that the iodido ligand is easily substituted is also apparent from the mass spectra of $ODN1^{PtI,GNA}$ and $ODN1^{PtI,DNA}$ (Fig. S3 and S4†), where the iodido ligand is found to be cleaved off.

Hence, in a second set of experiments, the iodido ligand was exchanged by a cyanido unit, which is expected to bind more tightly to the Pt(II) ion due to its strong σ-donor and π-acceptor character. This was again confirmed by mass spectrometry, where a non-dissociated Pt(II) complex was observed for $ODN1^{PtCN,GNA}$ and $ODN1^{PtCN,DNA}$ (Fig. S5 and S6†). Indeed, the **PtCN**-modified duplexes show a more regular melting behaviour, as illustrated in Fig. 1 based on duplexes $\mathbf{III}^{X}$. In the presence of the Pt(II) complex, a significant increase in T_m is observed with respect to the triazole-containing reference duplexes. The increase is largely independent of the complementary nucleobase (Fig. S7†), with duplex $\mathbf{II}^{PtCN,GNA}$ being a prominent exception. In general, the melting transition is steeper for duplexes in which the Pt(II) complex is attached *via* a 2′-deoxyribose, compared to the GNA linker. This is in agreement with the distortion expected upon the incorporation of the non-canonical backbone fragment. Again, the CD spectra indicate no major structural changes upon the introduction of the Pt(II) complex (Fig. 1b and S7†), except for the fact that the Pt(II)-free reference duplexes show an unusually strong positive Cotton effect at ∼280 nm. However, as the wavelengths of the

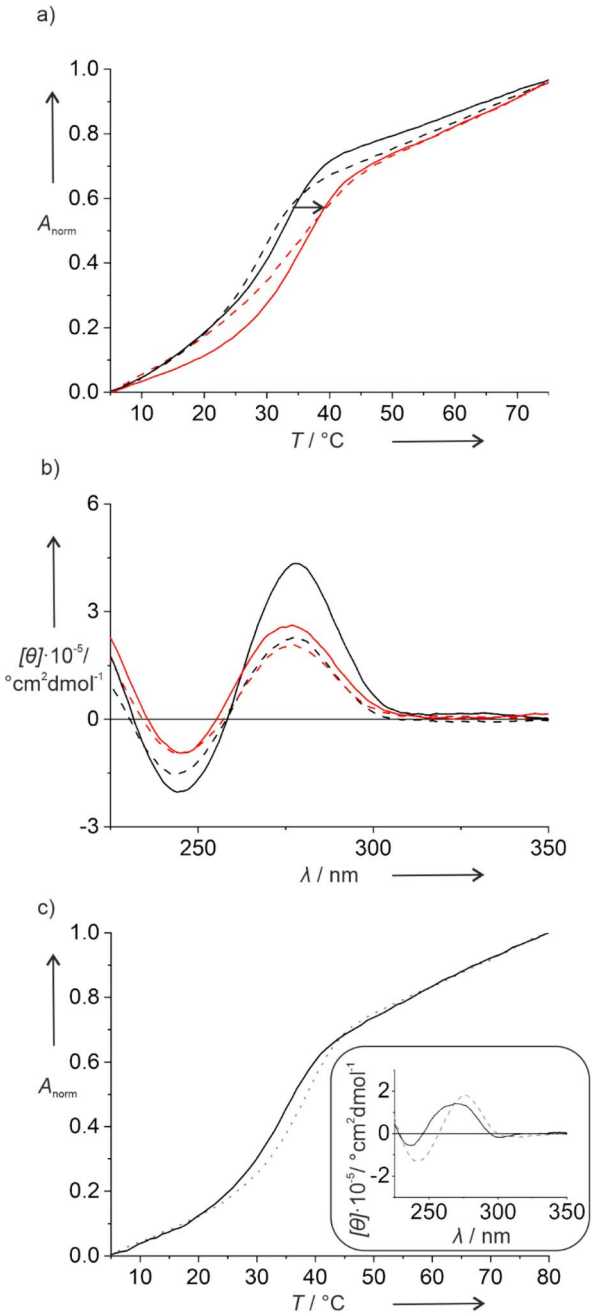

Fig. 1 (a) Melting curves and (b) CD spectra of duplexes $\mathbf{III}^{Tri,GNA}$, $\mathbf{III}^{PtCN,GNA}$, $\mathbf{III}^{Tri,DNA}$ and $\mathbf{III}^{PtCN,DNA}$. Broken lines represent the use of the GNA linker, solid lines of the DNA linker. Data for **PtCN**-containing DNA are shown in red, for the Pt(II)-free reference strands in black. (c) Melting curves of duplexes $\mathbf{I}^{PtCN,DNA}$ (dotted line) and **V** (solid line). The inset shows the corresponding CD spectra. Experimental conditions: 1 μM DNA duplex, 5 mM MOPS buffer (pH 7.0), 150 mM $NaClO_4$, 2.5 mM $Mg(ClO_4)_2$.

Cotton effects do not significantly shift in the presence of the Pt(II) complex, major structural changes can be ruled out.

Table 3 lists the melting temperatures of the duplexes in the presence of **PtCN**. The reason for the increased stabilization of duplex $\mathbf{II}^{PtCN,GNA}$ in comparison to the other duplexes with a **PtCN**, GNA modification remains unclear. While it could be

Table 3 Melting temperatures T_m/°C and change in melting temperature ΔT_m/°C compared to $\mathbf{I}^{Tri,GNA}$–$\mathbf{IV}^{Tri,GNA}$ and $\mathbf{I}^{Tri,DNA}$–$\mathbf{IV}^{Tri,DNA}$, respectively[a]

Duplex	T_m	ΔT_m	Duplex	T_m	ΔT_m
$\mathbf{I}^{PtCN,GNA}$	34.1	8.0	$\mathbf{I}^{PtCN,DNA}$	37.5	7.0
$\mathbf{II}^{PtCN,GNA}$	39.0	14.7	$\mathbf{II}^{PtCN,DNA}$	35.7	7.6
$\mathbf{III}^{PtCN,GNA}$	33.8	5.6	$\mathbf{III}^{PtCN,DNA}$	35.1	3.8
$\mathbf{IV}^{PtCN,GNA}$	34.1	9.1	$\mathbf{IV}^{PtCN,DNA}$	34.2	6.5

[a] Experimental conditions: 1 μM DNA duplex, 5 mM MOPS buffer (pH 7.0), 150 mM $NaClO_4$, 2.5 mM $Mg(ClO_4)_2$.

speculated that the complex optimally fits into a duplex with a complementary 2′-deoxycytidine, such an explanation would not be in agreement with the shallow melting transition (*vide supra*) or the data for **PtCN**, DNA.

To evaluate the effect of two consecutive Pt(II) complexes within a DNA double helix, duplex **V** was synthesized. It is derived from $\mathbf{I}^{PtCN,DNA}$ (the **PtCN**-containing duplex with the highest T_m) by formally replacing the T:A pair adjacent to the **X**:G pair by second **X**:G pair. Duplex **V** melts at 34.0 °C and hence at a slightly lower T_m as $\mathbf{I}^{PtCN,DNA}$ (Fig. 1c). Its CD spectrum resembles that of B-DNA. Nonetheless, slightly blue-shifted maxima with respect to those in the CD spectrum of duplex $\mathbf{I}^{PtCN,DNA}$ indicate a slight structural change upon the incorporation of the second Pt(II) complex (Fig. 1c).

The general applicability of our approach of a post-synthetic modification of nucleic acids with organometallic complexes was confirmed by applying the Pd(II) complex **PdCN** analogous to **PtCN**. As expected, the behaviour of the resulting duplexes is essentially identical, as exemplified by a comparison of the respective melting temperatures (Fig. S8, Table S1†).

Time-resolved photoluminescence spectroscopy

The photoluminescence spectra of the Pt(II)-containing oligonucleotides show an emission band peaking around 510 nm with a clear vibrational progression indicative of an emission from metal-perturbed ligand-centred states, in agreement with the results obtained for comparable complexes outside the DNA context (for representative examples, see Fig. S20–S24†).[29–31] The photoluminescence lifetimes are summarized in Table 4. They are in the order of μs and confirm that phosphorescent oligonucleotides were obtained. As the lifetimes also depend on the microenvironmental shielding of the Pt(II) complex from physical quenching by water and $^3O_2$,[37–39] they provide valuable structural information.

In the following, we will first discuss the behaviour in air-equilibrated solutions. Here, duplexes bearing **PtCN** entities in a complete DNA context have the longest amplitude-weighted average lifetimes, compared to **PtCN** attached *via* a GNA linkage and all **PtI**-containing duplexes. This means that in duplexes containing the oligonucleotide $ODN1^{PtCN,DNA}$, the Pt(II) complex is best shielded from water and dioxygen. The average lifetimes of the **PtCN** complexes attached *via* the uracil C5 position are shorter by 20–30% (see Fig. S9† for their melting curves and CD spectra and Table S2† for their T_m). Here, the Pt(II) complex is protruding into the major groove. It is therefore expected to be less efficiently shielded from water, which is in agreement with the shorter lifetimes. The poorer shielding in the single-stranded oligonucleotides ODN^X is reflected by their even further shortened lifetimes.

Upon Ar-purging, *i.e.,* in the absence of $^3O_2$, the lifetimes clearly reflect the different structural shielding from physical quenching. In general, they are always longer upon deoxygenation. The systems with **PtI** moieties show the shortest lifetimes, in agreement with a faster deactivation rate related to a lower ligand field splitting. The average lifetimes of **PtCN**-bearing duplexes are very similar, irrespective of the identity of the nucleobase in the complementary position and whether they are attached *via* a 2′-deoxyribose or a GNA linker. The duplexes with **PtCN** facing the major groove (*i.e.,* attached to uracil) display a somewhat shorter average lifetime (by 3–11%). Still, the duplex lifetimes remain longer than those of the corresponding single-stranded oligonucleotides, indicating that the complex is better shielded from quenching in the duplex. Taken together, these data are in agreement with the localization of the **PtCN** complexes either in the base pair stack or as groove binders. Even the shorter average lifetimes of all the DNA duplexes bearing **PtI** moieties reflect the different solvent and $^3O_2$ accessibility of their Pt(II) centres, in agreement with the non-specific cross-linking to other DNA strands as proposed above on the basis of the melting profiles.

Table 4 Amplitude-weighted average photoluminescence lifetimes τ/μs of the Pt(II)-containing DNA in solution, under air-equilibrated and de-aerated (*i.e.,* Ar-purged) conditions[a]

	Air-equilibrated					Argon-purged				
DNA	**PtI**,GNA	**PtI**,DNA	**PtCN**,GNA	**PtCN**,DNA	**PtCN**,Uri	**PtI**,GNA	**PtI**,DNA	**PtCN**,GNA	**PtCN**,DNA	**PtCN**,Uri
$ODN1^X$	5.3	5.9	4.3	4.9	6.2	11.6	13.2	19.5	20.7	19.8
$\mathbf{I}^X$	9.9	9.6	13.3	19.0	14.0	13.6	14.6	24.5	24.8	22.0
$\mathbf{II}^X$	7.7	9.3	13.6	16.6	11.6	13.8	14.4	23.9	23.6	21.4
$\mathbf{III}^X$	9.8	10.9	12.8	18.0	14.5	13.8	15.1	23.1	22.7	22.2
$\mathbf{IV}^X$	9.2	10.7	13.6	17.1	15.1	13.9	15.1	23.9	23.5	21.9

[a] Experimental conditions: 1 μM DNA (single-stranded in the case of $ODN1^X$, double-stranded for $\mathbf{I}^X$, $\mathbf{II}^X$, $\mathbf{III}^X$, $\mathbf{IV}^X$), 5 mM MOPS buffer (pH 7.0), 150 mM $NaClO_4$, 2.5 mM $Mg(ClO_4)_2$, room temperature, experimental uncertainty ± 0.1 μs. The corresponding original data, together with the fitting parameters, are given in the ESI (Fig. S25–S74).

The doubly platinated duplex **V** shows significantly different luminescent properties. Fig. 2 shows the photoluminescence spectra of this duplex and of the corresponding single-stranded ODN3 under different atmospheric conditions. In addition to the emission band with vibrational progression centring around 500 nm, a broad emission band is observed above 600 nm, indicating the presence of excimers. The average lifetimes of these excimeric species are significantly shorter than those of the monomers (Tables S3 and S4†). They are likewise shorter than those of the respective mono-platinated species $\mathbf{I}^{\mathbf{PtCN},\mathrm{DNA}}$ and $\mathrm{ODN1}^{\mathbf{PtCN}}$ (Table 4). In general, the lifetimes are reminiscent of what had been reported previously for a related Pt(II) complex interacting non-covalently with ctDNA *via* groove-binding.[40]

Interestingly, duplex **V** and single-stranded oligonucleotide ODN3 respond differently to the presence of dissolved molecular dioxygen. The luminescence intensity of the excimers above 600 nm is much less sensitive to dissolved dioxygen than that of the monomers at 500 nm. Thus, it could be used as an internal reference to sense the concentration of dissolved $^3O_2$, if compared with the monomeric emission (for clarity, the spectra shown in Fig. 2 have been normalized to the excimeric maximum peaking at *ca.* 620 nm). Interestingly, while the relative luminescence intensity of the monomer emission at 500 nm increases about 1.7-fold upon Ar-purging, this increase is much larger (3.2-fold) for the single strand, in agreement with an enhanced exposure to physical quenching. To confirm that this effect is due to the presence of dissolved $^3O_2$, the measurements were repeated by comparing Ar-purged to O_2-saturated solutions. Here, the relative monomer emission intensities increase 1.9-fold and 3.9-fold, respectively. Hence, the doubly platinated oligonucleotide $\mathrm{ODN3}^{\mathbf{PtCN}}$ (and to a lesser extent the corresponding duplex) constitutes an excellent candidate for a $^3O_2$ sensor based on the relative phosphorescence intensities of monomer and excimer (ratiometric quantification). On the other hand, while the average lifetimes of the green monomers are drastically prolonged upon de-oxygenation, the photoluminescence decays are less sensitive if monitored at the emission maximum of the red excimers. In fact, their relative ratios mirror the qualitative trend observed for the intensities, but the multi-exponential nature (Tables S3 and S4, Fig. S75–S86†) precludes a straightforward comparison (mainly due to the manifold of co-existing conformers), thus requiring the evaluation of amplitude-weighted average lifetimes.[41]

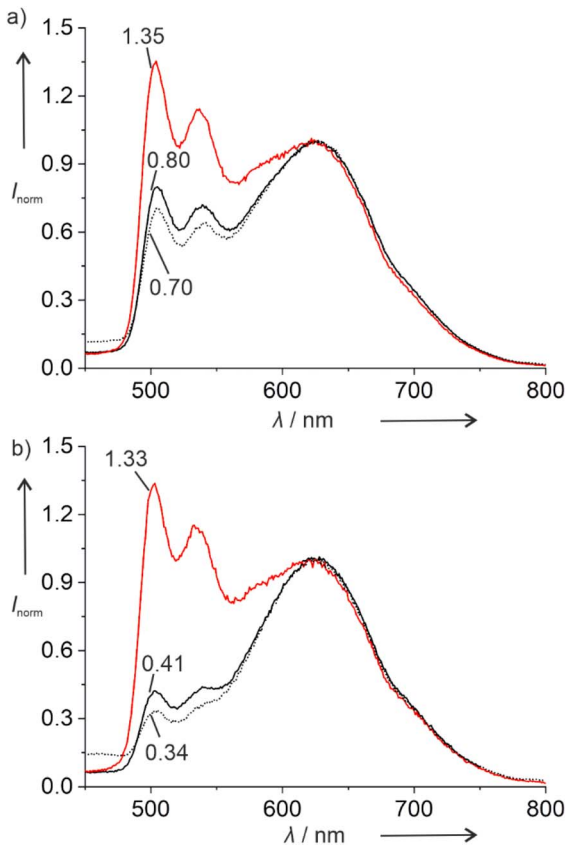

Fig. 2 Photoluminescence spectra and relative intensities of the monomers (with respect to the red-shifted excimers) of doubly platinated (a) duplex **V** and (b) single-stranded ODN3. Black solid line: air-equilibrated; red solid line: Ar-purged; black dotted line: O_2-saturated. Intensities normalized for clarity at (a) 625 nm and (b) 620 nm.

Conclusions

Tethering a phosphorescent tag to a nucleic acid is of high interest. Compared to commonly applied fluorophores,[42] a phosphorescent tag represents a tremendous advantage in anticipated *in vitro* experiments because of the suppression of background fluorescence in time-gated measurements. The Pt(II)-modified nucleic acids described here represent excellent candidates for such an application. We propose that they could serve as lifetime-based or ratiometric intensity $^3O_2$ sensors in aqueous solutions, broadening their scope by providing a dual readout for photoluminescence (lifetime imaging) microscopy. Future work will aim at establishing such an application in biological models and at introducing the Pt(II) complexes *via* shorter linkers, so that their location within the DNA can be predicted more precisely.

Data availability

Information supporting this article has been uploaded as part of the ESI.† The datasets generated during and/or analysed during the current study are available from the authors on reasonable request.

Author contributions

FB: investigation (synthesis, characterization); IM: investigation (photophysics); TS: investigation (synthesis); CAS, JM: supervision, conceptualization, funding acquisition; FB, IM, CAS, JM: Writing – original draft; Writing – review & editing.

Conflicts of interest

There are no conflicts to declare.

Acknowledgements

We thank Dr Marian Hebenbrock for fruitful discussions and for performing experiments at the onset of the project. We thank Dr Maria Victoria Cappellari for spectroscopic support. JM and CAS thank the Deutsche Forschungsgemeinschaft for funding (MU 1750/5-1, STR 1186/7-1, INST 211/915-1 FUGG).

Notes and references

1 E. Stulz and G. H. Clever, *DNA in supramolecular chemistry and nanotechnology*, John Wiley & Sons, Chichester, UK, 2015.
2 Z. J. Gartner, B. N. Tse, R. Grubina, J. B. Doyon, T. M. Snyder and D. R. Liu, *Science*, 2004, **305**, 1601–1605.
3 P. Ensslen and H.-A. Wagenknecht, *Acc. Chem. Res.*, 2015, **48**, 2724–2733.
4 H. Asanuma, T. Fujii, T. Kato and H. Kashida, *J. Photochem. Photobiol., C*, 2012, **13**, 124–135.
5 F. Hövelmann and O. Seitz, *Acc. Chem. Res.*, 2016, **49**, 714–723.
6 J. Gebhard, L. Hirsch, C. Schwechheimer and H.-A. Wagenknecht, *Bioconjugate Chem.*, 2022, **33**, 1634–1642.
7 Y. Takezawa, J. Müller and M. Shionoya, *Chem. Lett.*, 2017, **46**, 622–633.
8 S. Naskar, R. Guha and J. Müller, *Angew. Chem., Int. Ed.*, 2020, **59**, 1397–1406.
9 B. Lippert, *J. Biol. Inorg Chem.*, 2022, **27**, 215–219.
10 N. Santamaría-Díaz, J. M. Méndez-Arriaga, J. M. Salas and M. A. Galindo, *Angew. Chem., Int. Ed.*, 2016, **55**, 6170–6174.
11 H. Zhao, P. Leonard, X. Guo, H. Yang and F. Seela, *Chem. – Eur. J.*, 2017, **23**, 5529–5540.
12 I. Schönrath, V. B. Tsvetkov, T. S. Zatsepin, A. V. Aralov and J. Müller, *J. Biol. Inorg Chem.*, 2019, **24**, 693–702.
13 D. J. Hurley and Y. Tor, *J. Am. Chem. Soc.*, 1998, **120**, 2194–2195.
14 S. I. Khan, A. E. Beilstein and M. W. Grinstaff, *Inorg. Chem.*, 1999, **38**, 418–419.
15 M. D. Newton, S. D. Fairbanks, J. A. Thomas and D. S. Rueda, *Angew. Chem., Int. Ed.*, 2021, **60**, 20952–20959.
16 H. K. Saeed, S. Sreedharan and J. A. Thomas, *Chem. Commun.*, 2020, **56**, 1464–1480.
17 H. K. Saeed, P. J. Jarman, S. Archer, S. Sreedharan, I. Q. Saeed, L. K. Mckenzie, J. A. Weinstein, N. J. Buurma, C. G. W. Smythe and J. A. Thomas, *Angew. Chem., Int. Ed.*, 2017, **56**, 12628–12633.
18 B. Önfelt, P. Lincoln and B. Nordén, *J. Am. Chem. Soc.*, 2001, **123**, 3630–3637.
19 S. Le Gac, M. Foucart, P. Gerbaux, E. Defrancq, C. Moucheron and A. Kirsch-De Mesmaeker, *Dalton Trans.*, 2010, **39**, 9672–9683.
20 C. J. Murphy, M. R. Arkin, Y. Jenkins, N. D. Ghatlia, S. H. Bossmann, N. J. Turro and J. K. Barton, *Science*, 1993, **262**, 1025–1029.
21 D. Ukale, V. S. Shinde and T. Lönnberg, *Chem. – Eur. J.*, 2016, **22**, 7917–7923.
22 D. U. Ukale and T. Lönnberg, *ChemBioChem*, 2018, **19**, 1096–1101.
23 D. U. Ukale and T. Lönnberg, *Angew. Chem., Int. Ed.*, 2018, **57**, 16171–16175.
24 S. K. Maity and T. Lönnberg, *Chem. – Eur. J.*, 2018, **24**, 1274–1277.
25 S. K. Maity and T. Lönnberg, *ACS Omega*, 2019, **4**, 18803–18808.
26 D. U. Ukale, P. Tähtinen and T. Lönnberg, *Chem. – Eur. J.*, 2020, **26**, 2164–2168.
27 M. Hande, S. Maity and T. Lönnberg, *J. Inorg. Biochem.*, 2021, **222**, 111506.
28 K. Kowalski, *Coord. Chem. Rev.*, 2021, **432**, 213705.
29 M. Hebenbrock, L. Stegemann, J. Kösters, N. L. Doltsinis, J. Müller and C. A. Strassert, *Dalton Trans.*, 2017, **46**, 3160–3169.
30 M. Hebenbrock, D. González-Abradelo, A. Hepp, J. Meadowcroft, N. Lefringhausen, C. A. Strassert and J. Müller, *Inorg. Chim. Acta*, 2021, **516**, 119988.
31 I. Maisuls, F. Boisten, M. Hebenbrock, J. Alfke, L. Schürmann, B. Jasper-Peter, A. Hepp, M. Esselen, J. Müller and C. A. Strassert, *Inorg. Chem.*, 2022, **61**, 9195–9204.
32 B. Lippert, *Cisplatin - Chemistry and Biochemistry of a Leading Anticancer Drug*, Wiley-VCH and Verlag Helvetica Chimica Acta, Zürich, 1999.
33 R. Manchanda, S. U. Dunham and S. J. Lippard, *J. Am. Chem. Soc.*, 1996, **118**, 5144–5145.
34 J. Schliepe, U. Berghoff, B. Lippert and D. Cech, *Angew. Chem., Int. Ed. Engl.*, 1996, **35**, 646–648.
35 K. S. Schmidt, D. V. Filippov, N. J. Meeuwenoord, G. A. van der Marel, J. H. van Boom, B. Lippert and J. Reedijk, *Angew. Chem., Int. Ed.*, 2000, **39**, 375–377.
36 J. Hennessy, B. McGorman, Z. Molphy, N. P. Farrell, D. Singleton, T. Brown and A. Kellett, *Angew. Chem., Int. Ed.*, 2022, **61**, e202110455.
37 I. Maisuls, J. Singh, I. P. Salto, S. T. Steiner, T. M. Kirse, S. Niemann, C. A. Strassert and A. Faust, *Inorg. Chem.*, 2021, **60**, 11058–11069.
38 S. Chatnahalli Gangadharappa, I. Maisuls, I. P. Salto, S. Niemann, V. Bachtin, F. C. Herrmann and C. A. Strassert, *J. Phys. Chem. C*, 2021, **125**, 5739–5747.
39 I. Maisuls, C. Wang, M. E. Gutierrez Suburu, S. Wilde, C.-G. Daniliuc, D. Brünink, N. L. Doltsinis, S. Ostendorp, G. Wilde, J. Kösters, U. Resch-Genger and C. A. Strassert, *Chem. Sci.*, 2021, **12**, 3270–3281.
40 M. Hebenbrock, D. González-Abradelo, C. A. Strassert and J. Müller, *Z. Anorg. Allg. Chem.*, 2018, **644**, 671–682.
41 A. Sillen and Y. Engelborghs, *Photochem. Photobiol.*, 1998, **67**, 475–486.
42 S. Benson, F. de Moliner, W. Tipping and M. Vendrell, *Angew. Chem., Int. Ed.*, 2022, **61**, e202204788.